


Article

Synthesis of CaWO_4 as a Photocatalyst for Degradation of Methylene Blue and Carmine under Ultraviolet Light Irradiation

Cunyang Yuan^{1,2}, Fuwei Sun^{1,2}, Haibo Liu^{1,2}, Tianhu Chen^{1,2}, Ziyang Chu^{1,2}, Hanlin Wang^{1,2}, Xuehua Zou^{1,2}, Peixun Zhai^{1,2} and Dong Chen^{1,2,*} 

¹ Key Laboratory of Nano-Minerals, Pollution Control of Anhui Higher Education Institutes, Hefei University of Technology, Hefei 230009, China

² Institute of Environmental Minerals and Materials, School of Resources and Environmental Engineering, Hefei University of Technology, Hefei 230009, China

* Correspondence: cdxman@hfut.edu.cn

Abstract: Photocatalysis is considered a promising method for wastewater treatment; however, most synthesized photocatalysts have complex structures and are costly. Thus, in this study, a novel CaWO_4 sample was synthesized by a co-precipitation method in one step. The characteristic results show that CaWO_4 has good dispersibility, a large specific surface area, and good photoresponse under UV light. The synthesized CaWO_4 can be used to degrade methylene blue (MB) and carmine (CR) under UV light without the addition of oxidants. The effects of a water matrix, including pH value, solid–liquid ratio, light intensity, and initial concentration of pollutants on photocatalytic degradation were studied. According to the optimization of these factors, the optimal photocatalytic degradation condition was found under the catalyst concentration of 1.0 g/L and ultraviolet light intensity of 80 W. The optimal pH is 8.2 for the MB system and 6.0 for the CR system. The optimal photocatalytic degradation of MB and CR at 100 mg/L can be achieved as 100%. According to the results of scavenger experiments, holes and hydroxyl radicals dominate the degradation of MB while hydroxyl radicals and superoxide anions are mainly responsible for the degradation of CR. Further analyses showed that photogenerated electrons generated on the surface of the CaWO_4 can form electron–hole pairs, thereby producing hydroxyl radicals and superoxide anions to degrade dyes. In addition, the CaWO_4 has a good cycling performance in the process of degrading MB (more than 80% after five cycles). It provides a new idea for the photocatalytic degradation of dyes using mineral-like materials.

Keywords: dye; photocatalysis; calcium tungstate; free radical; mechanism



Citation: Yuan, C.; Sun, F.; Liu, H.; Chen, T.; Chu, Z.; Wang, H.; Zou, X.; Zhai, P.; Chen, D. Synthesis of CaWO_4 as a Photocatalyst for Degradation of Methylene Blue and Carmine under Ultraviolet Light Irradiation. *Processes* **2023**, *11*, 1050. <https://doi.org/10.3390/pr11041050>

Academic Editor: Andrea Petrella

Received: 19 February 2023

Revised: 21 March 2023

Accepted: 28 March 2023

Published: 31 March 2023



Copyright: © 2023 by the authors. Licensee MDPI, Basel, Switzerland. This article is an open access article distributed under the terms and conditions of the Creative Commons Attribution (CC BY) license (<https://creativecommons.org/licenses/by/4.0/>).

1. Introduction

With the rapid development of urbanization and industrialization, environmental pollution caused by a large number of dye-containing wastewater, such as textiles, leather, printing, plastic, food, medicine, cosmetics, and so on, has become a worldwide concern [1]. Dye wastewater usually has the characteristics of large amounts of organic matter and salts, as well as complex compositions. For example, cationic dyes are also known as basic dyes, because cationic dye wastewater is usually alkaline. This kind of dye has a bright color and high coloring power. It can ionize and produce positively charged ions after being dissolved in water. Aqueous solutions of anionic dyes are usually acidic and anionic dyes in water produce negatively charged ions. It is necessary to explore different experimental methods and reaction conditions to deal with different kinds of dyes [2].

Traditional physical, biological, and chemical treatment methods are difficult to use to treat dye wastewater [3]. The photocatalysis-based advanced oxidation process has the advantages of ease of operation, low energy consumption, no secondary pollution, and

high efficiency, and is considered a promising dye wastewater treatment technology [4,5]. The basic principle is that light makes electrons transition from the valence band to the conduction band under the excitation of ultraviolet light so that photogenerated electrons are concentrated in the conduction band, while the valence band of lost electrons forms a photogenerated hole. Electron–hole pairs have redox potentials and reduce oxygen to form superoxide anions and oxidize water to form hydroxyl radicals [6]. These free radicals work together to degrade pollutants in the water.

TiO₂ is considered one of the most promising photocatalysts [7]. Due to its advantages of environmental friendliness and ease of manufacturing, more and more researchers are devoted to the field of photocatalytic degradation of organic pollutants in water. However, there are still some problems in the photocatalytic application of TiO₂, such as the agglomeration effect, low photocarrier separation efficiency, and limited light absorption capacity, which lead to low catalytic efficiency of TiO₂ in a photocatalytic application.

Compared with the low band gap width of TiO₂, the band gap energy of g-C₃N₄ is only 2.7 eV, it has good photostability and chemical tunability [8]. In addition, the photocatalytic treatment of the dye by using the composite material with a thin coating of SiO₂ on TiO₂ as a catalyst has a good effect [9]. At the same time, novel catalyst materials, such as CaCu₃Ti₄O₁₂ with a surface local dipole moment and low band gap, are studied. Low band gap allows that catalyst separate carrier effectively in the photocatalytic process [10]; however, these composite photocatalytic processes also face many problems such as low efficiency, being nonvisible-light driven, complicated manufacturing, and high cost.

Fortunately, some raw mineral-based materials, because of their unique special properties such as high photocatalytic degradation efficiency, ease of operation, and environmental friendliness, were used instead of conventional TiO₂ and composite photocatalysis [11–13]. Herein, scheelite (CaWO₄) can be used for excellent photocatalysis in recent years due to its unique light response characteristics. Nano CaWO₄ has good dispersion, high light absorption, and a low photoelectron–hole pair recombination ratio. CaWO₄ has good photoluminescence under UV light and is a good direct semiconductor catalyst. The appropriate band gap width will neither hinder the excitation of electrons nor hinder the recombination with electrons, which is beneficial to the continuous progress of the photocatalytic reaction. In the treatment of dye wastewater, CaWO₄ is insoluble in various dye solutions and will not adsorb dye, so it can be efficiently recycled. Therefore, it is considered a kind of photocatalyst with broad application prospects.

Some studies show that the performance of scheelite as a catalyst is good after doping modification. BaMoO₄-coupled CaWO₄ heterojunction micro/nanocomposites can effectively improve the photocatalytic ability of catalysts by improving the photoelectron excitation but the preparation method of the catalysts is complicated [14]. In addition, the use of natural materials to prepare catalysts is also an important development direction. It is an environmentally friendly method to prepare the photocatalyst SrO from plant extracts by coprecipitation. Because plant extracts can better control the particle size, morphology, and structure of the SrO, the catalytic performance of the catalyst can be improved. The degradation efficiency can be increased by 87.4% in the photocatalytic system with MB as the target pollutant by performance optimization [15].

In this study, the work focuses on the issues of as-prepared CaWO₄ and its catalytic activity. Nano-CaWO₄ was prepared in one step by a simple coprecipitation method. In the system of degradation of pollutants using CaWO₄ as the photocatalyst, the pollutants could be degraded by direct ultraviolet irradiation without doping modification. In addition, no oxidant is needed in this process, and the degradation effect can achieve the goal of almost complete removal of pollutants. Compared with previous reports, no doping of the modified catalyst and no addition of oxidants are needed to make the reaction simpler and more feasible. The aims of this paper can be summarized as follows: (1) The preparation and characterization of novel CaWO₄ catalysts equipped with preferable photocatalytic ability; (2) The optimized conditions of photocatalytic degradation of dyes; (3) The mechanism of CaWO₄ photocatalysis degradation of dyes.

2. Experimental Methods

2.1. Chemicals

All chemicals were of analytical grade unless otherwise noted.

MB and CR were purchased from Fuchen (Tianjin, China) Chemical Reagents Co., Ltd. (Shanghai, China). Ethylenediaminetetraacetic acid disodium salt (EDTA-2Na), tert-butanol (TBA), Tiron, NaF, Calcium chloride (CaCl_2), sodium tungstate (Na_2WO_4), cetyl trimethyl ammonium bromide (CTAB), n-butanol, n-octane, disodium hydrogen phosphate, and sodium dihydrogen phosphate were purchased from Sinopharm Group Chemical Reagent Co., Ltd., Shanghai, China. During the experimental process, ultrapure water ($18.2 \text{ M}\Omega\text{-cm}$) was used for preparing solutions.

2.2. Preparation Catalyst

Preparation of CaWO_4 photocatalyst followed the following steps. CaCl_2 solution at 0.5 mM concentration and Na_2WO_4 solution at 0.5 mM concentration were first added to a mixture of CTAB, n-butanol, and n-octane and stirred for 30 min. Then, the mixture was stirred for 5 min before it was left to rest for 6 h. CaCl_2 and Na_2WO_4 constitute a CaWO_4 inorganic core, while CTAB, n-butanol, and n-octane indicate a shell. Finally, the supernatant was centrifuged and the precipitate was washed and dried to obtain the CaWO_4 [16]. The process of catalyst preparation is shown in Figure S1a,b.

2.3. Catalyst Characterization

The phase and composition of the as-prepared samples were measured by X-ray diffraction (XRD, DS-2700, Dandong, China) using an X-ray diffractometer with $\text{Cu K}\alpha$ radiation under 40 kV and 100 mA and with a 2θ ranging from 10° to 70° . The morphologies and microstructures of the as-prepared samples were investigated by transmission electron microscopy (TEM, JEM-2100F, Japan). The element mapping of the samples was performed during the TEM measurements. UV–Vis diffuse reflectance spectra (DRS) of the samples were recorded with a UV–Vis spectrophotometer (Evolution220, Thermo Scientific, Waltham, MA, USA). Thus, the wavelength range of light absorbed by the sample was explored. Surface area analysis equipment (NOVA-3000e, USA) was used to analyze the specific surface area and porosity of the catalyst. The BET-specific surface of the catalysts was measured by the N_2 adsorption–desorption isotherms at -196°C on an adsorption unit (Novawin 3000e), and the pore volume, mean particle size, and pore diameter were determined by Barrett–Joyner–Halenda (BJH) method from desorption branches of the isotherms. To investigate the production of photogenic electrons, electrochemical workstation was used to detect the photoelectrical response of the catalyst. Zeta potential (Nano ZS90, UK) analyzer was used to determine the potential of solution after sample dissolution and the value of isoelectric point.

2.4. Photocatalytic Degradation of MB and CR

Photocatalytic activities of the calcium tungstate photocatalyst were evaluated by photocatalytic degradation of MB/CR under a lamp with adjustable light intensity as the light source (PLS-LED100B, Perfectlight, Beijing, China). By adjusting the reaction device, the distance between the liquid level and the light source is 5 cm. In order to detect whether the light source will heat the reaction solution, the temperature of the solution was detected by using a temperature gun during the reaction process (Figure S2). The result that the solution temperature varies within 10°C suggests that reaction temperature difference is in negligible amounts of the photocatalytic reaction. The experiments were performed at room temperature as follows: CaWO_4 was added into MB solution or CR solution. The solid–liquid ratios of photocatalyst and solution are 1 g/L, 0.8 g/L, 0.6 g/L, 0.4 g/L, and 0.2 g/L, respectively. The concentration of MB solution and CR solution used was 30 mg/L, 50 mg/L, 100 mg/L, and 200 mg/L, respectively. The pH was controlled by adding 0.01 mol/L HNO_3 or NaOH solution. Prior to irradiation, the suspensions were magnetically stirred for an hour in the dark to ensure the adsorption/desorption

equilibrium between photocatalyst powders and MB and CR. When photocatalytic reaction was triggered, 2 mL aliquot was taken out from reactor at intervals of every 30 min. The samples were tested after passing through the membrane. The concentration of MB was determined using a UV–Vis (Evolution220, Thermo Scientific, USA) spectrophotometer at its maximum absorption wavelength of 665 nm; the concentration of CR was determined using a UV–Vis spectrophotometer at its maximum absorption wavelength of 495 nm. It is worth mentioning that the color of CR solution varies with pH [17]. Therefore, before using UV–Vis spectrophotometer to detect CR solution, it is necessary to use pH buffer of disodium hydrogen phosphate and sodium dihydrogen phosphate mixed configuration to buffer carmine solution. The total organic carbon (TOC) was measured by Multi N/C 3000 TOC analyzer (Analytikjena, Jena, Germany). Surface functional groups of samples before and after reaction were analyzed by Fourier-transform infrared spectroscopy (FT-IR, VERTEX 70, Bruker, Billerica, MA, USA). For the cycle experiments, after each reaction, the used sample was centrifuged and washed with deionized water. After that, samples were dried and tested under the same experimental conditions. This process was repeated 5 times to test the reusability of the samples.

3. Result and Discussion

3.1. Characterization

The XRD patterns of CaWO_4 are shown in Figure 1a. The reflections at $2\theta = 18.60^\circ$, 28.72° , 31.44° , 34.17° , 39.20° , 47.10° , 54.30° , and 58.05° are corresponded to scheelite (JCPDS#41–1431). The results indicated that the as-synthesized sample is scheelite (CaWO_4) [18]. In addition, due to the use of organic matter in the synthesis process, washing with pure water and ethanol is difficult to completely remove organic matter residues, so the resulting sample may contain small amounts of residual impurities.

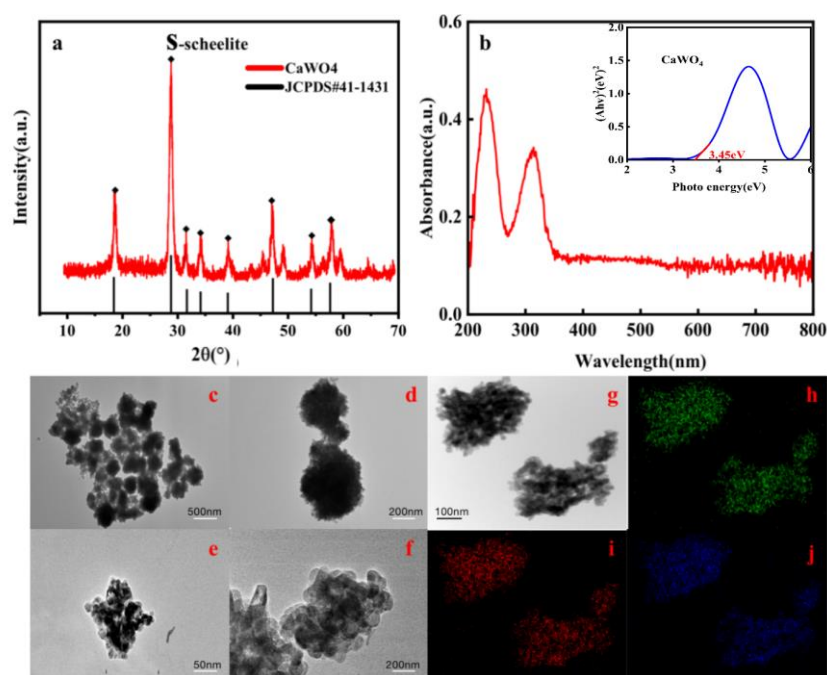


Figure 1. (a) XRD patterns of CaWO_4 ; (b) UV–Vis DRS spectra of CaWO_4 ; (c–g) TEM images of CaWO_4 ; (h–j) Element mapping images of Ca, W, and O.

To investigate the morphology and structure of CaWO_4 samples, TEM was further carried out and the results are shown in Figure 1c–f. It can be indicated that the synthesized CaWO_4 samples were granular and the particle size of the sample was between 20 and 30 nm. According to the TEM-based mapping analysis (Figure 1g–j), W, O, and Ca are evenly distributed, indicating from another angle that CaWO_4 was successfully prepared.

In addition, according to the calculation of element proportion (Figure S3), the element distribution conforms to the CaWO_4 molecular formula [19].

The photoresponse characteristics of the catalysts were characterized by UV–Vis DRS. As illustrated in Figure 1b, the absorption onset of nano- CaWO_4 was around 400 nm, corresponding to the band gap energy (E_g) of 3.45 eV. In the wavelength range below 400 nm, the absorption capacity of the sample is good, especially at 240 nm and 330 nm. The result explains why the light absorption capacity of CaWO_4 under ultraviolet light is stronger than that under visible light.

The adsorption volume and pore size distribution of catalysts also have important effects on catalytic performance. As can be seen in Figure S4a,b, the nitrogen adsorption–desorption isotherms of CaWO_4 showed a type IV isotherm and type H_3 hysteresis loops, indicating that the samples possessed a high proportion of mesopores and the pore shape belonged to slit-shape. In addition, the pore size distribution of CaWO_4 shows that CaWO_4 samples are mainly composed of 2–4 nanoparticles. The BET-specific surface of CaWO_4 is $76.44 \text{ m}^2/\text{g}$. The conclusion can be drawn that the adsorption capacity and pore size distribution of CaWO_4 samples are favorable for the catalytic reaction [20].

Hence, through the characterization, it can be seen that nano- CaWO_4 material was synthesized by a simple coprecipitate method. The sample has good dispersibility, a large specific surface area, and good photoresponse performance under UV light. Deservedly, samples were used for photocatalytic experiments.

3.2. Degradation of MB

3.2.1. Comparison Experiment and TOC Removal

The photocatalytic degradation of MB was verified by comparison experiments. Figure S5 demonstrates that the MB was hardly removed under UV irradiation or bare CaWO_4 , with a degradation efficiency of about 15% in 3 h. It indicates the adsorption of CaWO_4 and the photolysis of MB could be ignored. In contrast, in the presence of CaWO_4 and UV irradiation, 100 mg/L of MB could be completely degraded in 3 h. This shows that CaWO_4 has superior photocatalytic degradation efficiency of MB without adding oxidants [21]. As seen in Figure S6, the TOC removal efficiency reached 58% after a 3 h reaction when the MB removal efficiency was 99%, which indicates that the mineralization rate of pollutants is moderate. The reason why the mineralization efficiency is lower than the degradation efficiency may be due to the intermediates produced in the degradation process of MB rather than the complete conversion of CO_2 and H_2O .

3.2.2. Effect of Reaction Conditions

The photocatalytic degradation of MB is affected by different reaction conditions. The effects of the solid–liquid ratio, light intensity, pollutant concentration, and initial pH values on the degradation of MB were investigated and the results are illustrated in Figure 2a–d. It is well-known that the increase in solid–liquid ratio and light intensity can promote the degradation of pollutants in the photocatalytic reaction process [22]. When the solid–liquid ratio increased from 0.2 g/L to 1.0 g/L, the MB degradation efficiency was promoted from 69% to 96% in 180 min. In addition, when the light intensity increased from 20 W to 80 W, the MB degradation efficiency was promoted from 26% to 96%. Then, increasing the concentration of contaminants caused a decline in the degradation rate. When the concentration of MB is 200 mg/L, its degradation efficiency is only 25%, and when the concentration of MB is 30 mg/L, 50 mg/L, and, 100 mg/L, its degradation efficiency can reach more than 96%. Interestingly, the influence of pH on MB is not linear [23]. The maximum MB degraded rate appeared at a pH of 8.2, and the rate was reduced when the pH value rose above or dropped below 8.2. This may be due to the MB solution itself containing cationic dye ionization in water formed by positive ions [24]. The positively charged ions are attracted to the photogenerated electrons, which inhibits the recombination of electron–hole pairs and promotes the photocatalytic reaction effect. Therefore, under the original pH condition of the MB solution, the optimal MB degradation degree is obtained.

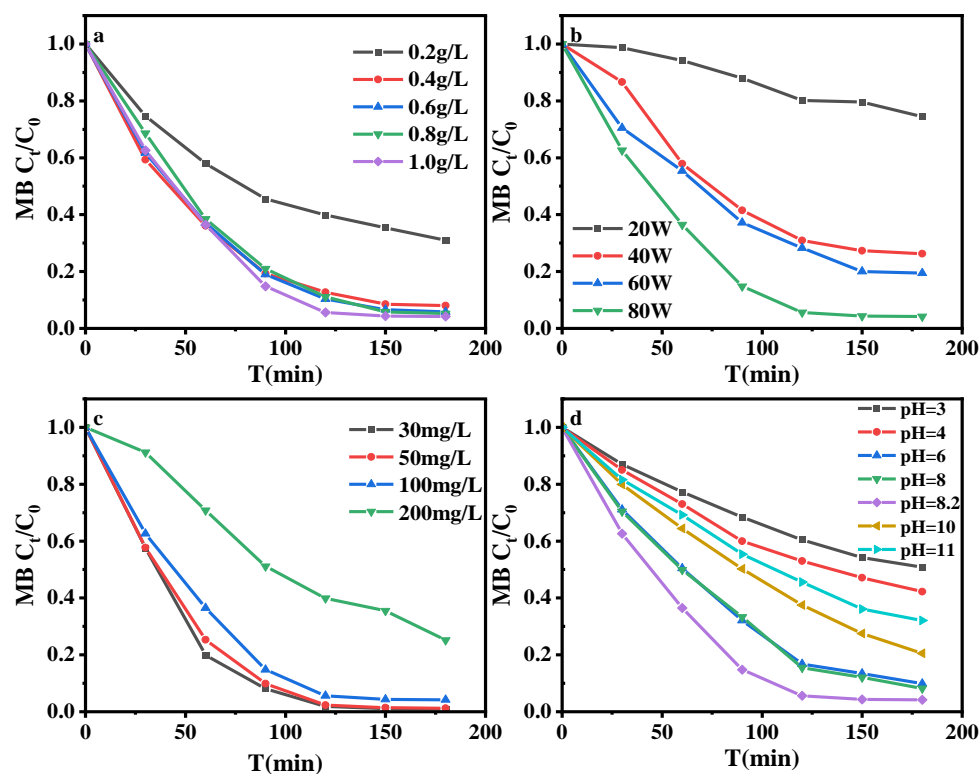


Figure 2. Effects of (a) Solid–liquid ratio; (b) Light intensity; (c) MB concentration; and (d) initial pH on MB removal efficiency. Reaction conditions: light intensity = 80 W; [MB] = 100 mg/L; pH = 8.2 for (a), [CaWO₄] = 1.0 g/L; [MB] = 100 mg/L; pH = 8.2 for (b), [CaWO₄] = 1.0 g/L; light intensity = 80 W; pH = 8.2 for (c), and [CaWO₄] = 1.0 g/L; light intensity = 80 W; [MB] = 100 mg/L for (d).

3.2.3. Identification of Reactive Species

To investigate the mechanism of MB degradation via CaWO₄, different scavengers were introduced to the system to identify and investigate the working reactive oxygen species (ROS). According to previous studies, in the process of photocatalytic degradation of organic contaminants, four active substances are chiefly involved: electrons, holes, hydroxyl radicals, and superoxide radicals [25]. In this study, EDTA-2Na, TBA, Tiron, and NaF were utilized to verify the contribution of h⁺, ·OH, O₂[−], and e[−], respectively. Figure 3a–d shows the influence of different quenchers on the experimental effect. Firstly, photoexcited electron transitions produce photogenerated electrons. However, the addition of 0.5 mM, 1.0 mM, and 5.0 mM NaF has little effect on MB degradation, indicating that electrons do not play a role in the photocatalytic degradation of MB. Then, photoexcited electron transitions leave electron holes. EDTA-2Na, an effective scavenger, was employed to scavenge as its role. It shows a high reactivity towards the holes. When 0.5 mM EDTA-2Na was used, photocatalytic degradation of methylene blue was suppressed. When the concentration of EDTA-2Na rose from 0.5 mM to 5.0 mM, the degradation efficiency of MB was reduced from 75% to 51%. It suggests that holes play an important role in photocatalysis. Then, water is oxidized to produce hydroxyl radicals. It is widely accepted in studies that alcohols without an alpha-hydrogen, such as tert-butanol, are one of the best scavengers of hydroxyl radicals [26]. After adding TBA, the photocatalytic effect becomes worse. The degradation efficiency of MB was inhibited by only 40% when 0.5 mM TBA was added. When TBA concentration reached 5.0 mM, the degradation efficiency of MB was inhibited by only 45%. Obviously, the degradation efficiency of MB was inhibited by TBA. This indicates that hydroxyl radicals are one of the key radicals in the degradation of MB. The active species in the reaction system also include the superoxide anion produced by the reduction in oxygen. Tiron was selected for quencher of O₂[−] [27,28]. According

to the results, the quenching of Tiron has an effect on photocatalysis but the effect is not significant. When the added Tiron concentration was increased from 0.5 mM to 5.0 mM, the degradation rate of MB decreased from 22% to 30%, respectively. Tiron inhibited the degradation of a small amount of MB. This indicates that superoxide anions also participate in the photocatalytic degradation of MB to a certain extent.

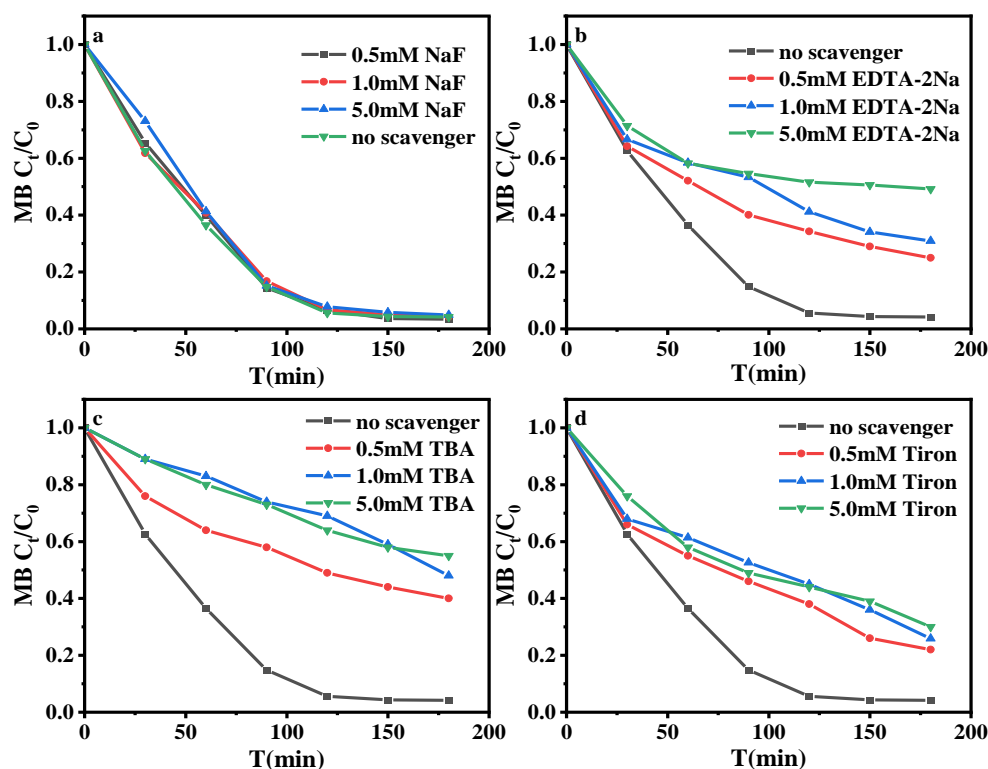


Figure 3. Effect of (a) NaF; (b) EDTA-2Na; (c) TBA; and (d) Tiron quenching agent on MB removal efficiency. Reaction conditions: light intensity = 80 W; [MB] = 100 mg/L; and pH = 8.2; [CaWO₄] = 1.0 g/L.

As a consequence, holes and hydroxyl radicals dominate the photocatalytic degradation of MB, and superoxide anions are also partly responsible for MB degradation, while electrons are not involved in this process.

3.3. Degradation of CR

3.3.1. Comparison Experiment and TOC Removal

The degradation of MB by CaWO₄ was studied. Consider that cationic dyes are stable. Positively charged ions generated by the ionization of cationic dyes attract photoelectrons and promote photocatalytic reactions. Therefore, in order to further explore the degradation ability of CaWO₄ on dyes, the unstable anionic dye CR, which ionizes and generates negative ions to interfere with photocatalytic reactions, was selected for the experiment. The photocatalytic degradation of CR was verified by a comparison experiment. As seen from Figure S8, CR was hardly removed under the condition of only UV light or CaWO₄, with a degradation efficiency of about 20% within 3 h. It indicates that the adsorption of CR by CaWO₄ and the photolysis of CR are both at a low level. In contrast, in the presence of CaWO₄ and UV irradiation, 100 mg/L of CR can be completely degraded in 3 h. The results show that CaWO₄ has good photocatalytic degradation of CR without an oxidizing agent. The TOC removal efficiency reached 42% after the reaction for 3 h when the CR removal efficiency was 99%, as displayed in Figure S9. It indicates that the mineralization efficiency of pollutants is relatively low. Only a small part of CR is converted to CO₂ and H₂O during photocatalytic degradation.

3.3.2. Effect of Reaction Conditions

The photocatalytic degradation of CR was affected by different reaction conditions. Effects of the solid–liquid ratio, light intensity, pollutant concentration, and initial pH values on CR degradation were shown in Figure 4a–d. There is a clear trend, when the solid–liquid ratio and light intensity increased, the degradation effect of CR improved [29]. When the solid–liquid ratio increased from 0.2 g/L to 1.0 g/L, the CR degradation was efficiency promoted from 72% to 99%. In addition, when the light intensity increased from 20 W to 80 W, the degradation efficiency of MB increased from 24% to 99%. In contrast, when the carmine concentration increased, the photocatalytic effect became worse. When the concentration of CR was 200 mg/L, the degradation efficiency was only 36%, while when the concentration of CR was reduced to 30 mg/L, 50 mg/L, or 100 mg/L, the degradation efficiency was above 99%. These are some common rules. Interestingly, the degradation efficiency of CR was highest at a pH of 6 [30]. When pH was 4 or 8, CR degradation efficiency remained high but when pH was 3 or 9, CR degradation efficiency was significantly lower. This may be due to the maximum positive potential of calcium tungstate solution at a pH of 6, reaching 2 mV. In this case, positively charged ions will attract photogenerated electrons, reducing the recombination of electron–hole pairs, thus promoting the effect of photocatalysis. When the pH is too low or too high, especially at a pH of 3 or 9, the potential of the CaWO_4 solution is very negative, at -26 mV and -15 mV, respectively (Figure S10). At this time, negatively charged ions will repel photogenerated electrons and accelerate the recombination of electron–hole pairs, thus reducing the photocatalytic effect.

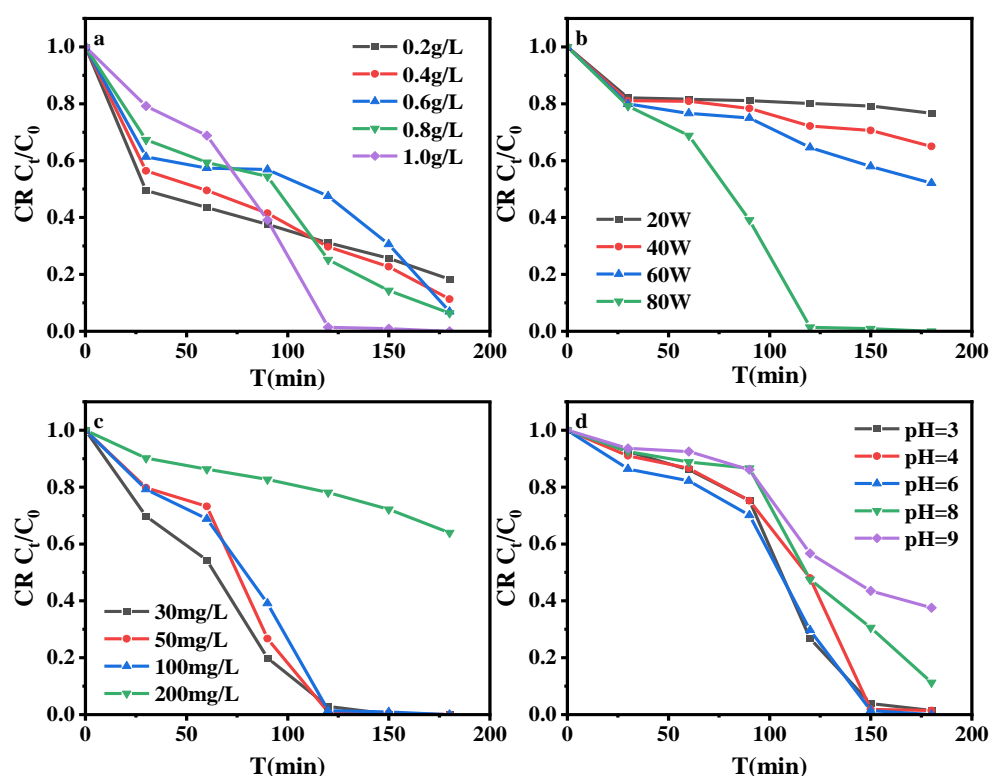


Figure 4. Effects of (a) Solid–liquid ratio; (b) Light intensity; (c) CR concentration; and (d) initial pH on CR removal efficiency. Reaction conditions: light intensity = 80 W; $[\text{CR}] = 100$ mg/L; pH = 6 for (a), $[\text{CaWO}_4] = 1.0$ g/L; $[\text{CR}] = 100$ mg/L; pH = 6 for (b), $[\text{CaWO}_4] = 1.0$ g/L; light intensity = 80 W; pH = 6 for (c), and $[\text{CaWO}_4] = 1.0$ g/L; light intensity = 80 W; $[\text{CR}] = 100$ mg/L for (d).

3.3.3. Identification of Reactive Species

To further study the participation of various active species in CR degradation, e^- , h^+ , $\cdot\text{OH}$, and O_2^- quenching experiments were employed in this study [31] because these

four kinds of active species are the main active substances produced in the photocatalytic process [32,33]. The effects of these quenching experiments on the photocatalytic degradation of CR are depicted in Figure 5a–d. First, photogenerated electrons are created in the presence of a photoexcited catalyst. However, electrons do not play a role in the photocatalytic degradation of CR because the degradation effect of CR was not affected when NaF was used as a quenching agent; the degradation of CR was not affected when 0.5 mM, 1.0 mM, and 5.0 mM NaF was added to the reaction system. Secondly, the electrons create holes after their transition. EDTA-2Na was used to quench holes, which slightly influenced the degradation of CR. When the concentration of EDTA-2Na was 0.5 mM and 1.0 mM, CR degradation was almost unaffected. When the concentration of EDTA-2Na was increased to 5.0 mM, the degradation efficiency of CR was reduced by 28%. It can be seen that holes are involved in photocatalytic reactions but are not major participants. In addition, hydroxyl radicals are produced when water is oxidized. The TBA hydroxyl radical quenching experiment shows a significant effect on the experimental results. When 0.5 mM TBA was used as a quencher, the photocatalytic degradation efficiency of CR was reduced by 36%. When the concentration of TBA was increased to 1.0 mM and 5.0 mM, the degradation of CR was inhibited more obviously, and the degradation efficiency of CR was reduced by 42% and 55%, respectively. This indicates that hydroxyl radicals are the main participant in the CR degradation reaction. The superoxide anions produced by oxygen reduction are also important active species. This is because the addition of Tiron to the reaction system to quench superoxide ions had a significant inhibition effect on the degradation of CR. For 0.5 mM and 1.0 mM Tiron, this reduced the degradation efficiency of CR by 35% and 36%, respectively. In addition, Tiron of 5.0 mM reduced the CR degradation efficiency by 56%.

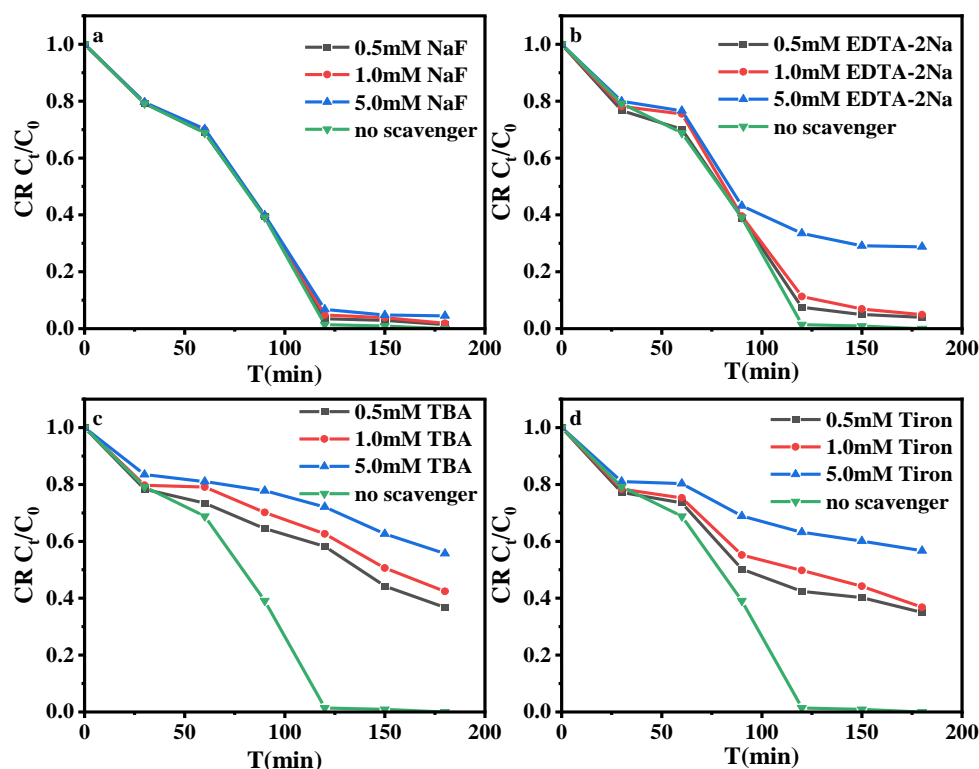


Figure 5. Effect of (a) NaF; (b) EDTA-2Na; (c) TBA; and (d) Tiron quenching agent on CR removal efficiency. Reaction conditions: light intensity = 80 W; [CR] = 100 mg/L; and pH = 8.2; [CaWO₄] = 1.0 g/L.

As a consequence, hydroxyl radicals and superoxide anions dominated the photocatalytic degradation of CR, and holes were also involved partly in the reaction, while electrons were almost not involved in the reaction.

3.4. Photocatalytic Activity

The removal of pollutants by photocatalysis is one of the hot research issues. The ZnO synthesized by hydrothermal methods at 200 °C is considered to be a good catalyst due to its more defective structures on the surface, which can achieve a maximum degradation rate of 91% of MB within 180 min [34]. Furthermore, modification of the catalyst is more beneficial to its catalytic performance. Magnetically retrievable Cobalt-doped ZnO nanowires are considered to be excellent photocatalysts. The 8% cobalt-doped ZnO nanowires can photocatalyze the degradation of Methyl Orange (MO) up to 93% within 180 min [35]. The construction of novel g-C₃N₄-coupled efficient Bi₂O₃ nanoparticles is also an important improvement on the photocatalytic effect, which can degrade 88.5% Rhodamine B (Rh B) in 180 min [36]. In addition, the morphology of the catalyst is also very important for the catalytic performance. Porous sponge-like CeO₂ morphology is helpful to the improvement of catalytic performance. The porous CeO₂ exhibited the highest activity, with a degradation of Methyl Green (MG) of 40% in 120 min, which is about twice the removal efficiency of the same type of commercial catalyst [37]. In addition, adding an oxidant is one of the important ways to improve the photocatalytic effect. Bi₂O₃-TiO₂ materials with peroxydisulfate synergistic action have high photocatalytic capacity. In this system, the photocatalytic degradation of Sulfamethoxazole (SMZ) can be 97.96% within 120 min [38]. There are also relevant studies on CaWO₄ materials. Using Ag₂MoO₂- and α -AgWO₄-doped CaWO₄, photocatalytic degradation of MB can achieve a degradation rate of 91.4% and 85.84% in 180 min and 105 min, respectively [39,40]. The degradation performance of different catalysts (1 g/L) for pollutants is shown in Table 1.

Table 1. Photocatalytic performance of different materials.

Material	Doping	Oxidant	Efficiency
ZnO	undesired	undesired	91% (5 mg/L MB) within 180 min
Co-ZnO	requisite	undesired	93% (10 mg/L MO) within 180 min
g-C ₃ N ₄ /Bi ₂ O ₃	requisite	undesired	88.5%(16.6 mg/L Rh B) within 180 min
CeO ₂	undesired	undesired	40% (10 mg/L MG) within 120 min
Bi ₂ O ₃ -TiO ₂	requisite	PDS (1 g/L)	97.96% (100 mg/L SMZ) within 120 min
CaWO ₄	undesired	undesired	98% (100 mg/L MB) within 180 min
CaWO ₄ /Ag ₂ MoO ₂	requisite	undesired	99% (100 mg/L CR) within 180 min
CaWO ₄ / α -AgWO ₄	requisite	undesired	91.4% (40 mg/L MB) within 180 min
			85.84%(200 mg/L MB) within 105 min

3.5. Study on Photocatalytic Mechanism

It is well-known that photocatalysis transfers electrons to jump from the valence band to the conduction band under ultraviolet light to create electron–hole pairs [41]. The electron–hole pair has the ability to redox, which degrades the pollutant. Therefore, the production of photogenerated electrons is an important part of the photocatalytic reaction. In order to explore the photocatalytic degradation mechanism of MB and CR by CaWO₄, the photoelectric response performance of CaWO₄ material was detected. The *i*-*t* curve of CaWO₄ was measured by an electrical workstation and the results are shown in Figure 6a. It is obvious that the generation of current is related to the irradiation of the light source. When the light is turned on and off at the same time interval, the generation and disappearance of current also change regularly with the light source being turned on and off. When the lamp is turned on, a large number of electrons generate a current. At this time, the direction of the current is denoted as the positive direction, and the current value is positive. When the lamp is turned off, the electrons annihilate and the instant current in the opposite direction is generated. At this time, the current value is negative. These results indicate that CaWO₄ is a preferable photocatalyst material with a superior photoelectric response ability. Under ultraviolet light, CaWO₄ will rapidly produce a large number of electron transitions, which means it will form a large number of electron–hole pairs, and then participate in the photocatalytic degradation of pollutants.

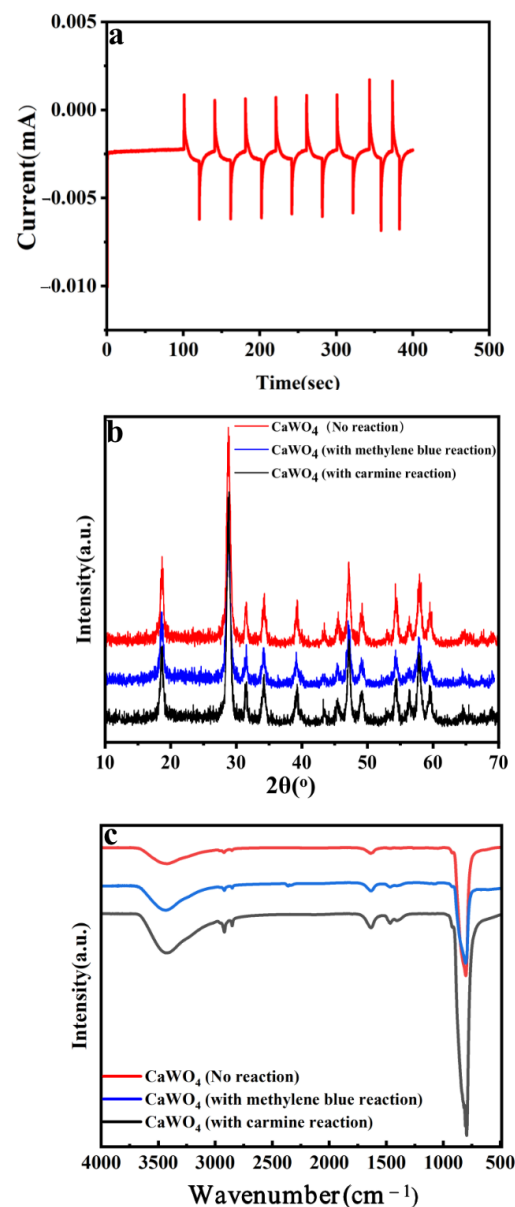


Figure 6. (a) I-t curves obtained at 0.0 V where 100 mM Na₂SO₄ was used as electrolyte; (b) XRD patterns of CaWO₄ (no reaction), CaWO₄ (with MB reaction), and CaWO₄ (with CR reaction); (c) FT-IR spectra of CaWO₄ (original sample), CaWO₄ (after reaction with MB), and CaWO₄ (after reaction with CR).

As depicted in Figure 6b, XRD diffraction peaks before and after reactions do not change significantly, indicating that the adsorption amounts of dyes are negligible. The main reaction process is through the degradation of pollutants. A similar situation can be found in the FT-IR spectrum. As shown in Figure 6c, the functional groups of the samples before and after the reaction were investigated using FT-IR spectroscopy. In the FT-IR spectra of CaWO₄ before and after the reaction, a broad absorption peak at around 3500 cm⁻¹ contributed to the stretching vibration of the physically adsorbed water molecule [42]. In addition, the bands at around 2900 cm⁻¹, 1500 cm⁻¹, 760 cm⁻¹, and 490 cm⁻¹ were assigned to the stretching vibrations of O-H, H-O-H, O-W-O, and W-O bonds, respectively. In addition, it is not difficult to see that the characteristic absorption peaks of samples do not change significantly before and after the reaction. The characteristic absorption peaks of MB and CR were not obvious in the samples after the reaction. That is to say, the characteristic absorption peaks of MB and CR do not appear in the samples

after the reaction. This indicates that the adsorption capacity of CaWO_4 on MB and CR is in negligible amounts through the photocatalytic reaction process. The degradation of MB and CR is the main process of photocatalysis.

3.6. Reusability of CaWO_4

The reusability of the activators is vital for actual applications [43]. Thus, cycle experiments were conducted to investigate the stability of CaWO_4 . As seen in Figure 7a,b, the reusability of CaWO_4 in photocatalytic degradation of MB and CR was verified. As for MB degradation, after five cycles, the material did not exhibit obvious deactivation, and the MB degradation efficiency is still more than 80%. It suggests that CaWO_4 can be reused in the photocatalytic degradation of MB. However, in the case of carmine, after the same five cycles, the activity of the CaWO_4 decreased significantly and the CR degradation efficiency only reached 48%. This suggests that CaWO_4 is not recommended to reuse more than three times in the photocatalytic degradation of CR. The different reusability exhibition in the degradation experiments of MB and CR is attributed to the different properties of MB wastewater and CR wastewater. The key to the degradation of MB and CR is to stimulate the electron transition in the catalyst to form electron–hole pairs, and further generate hydroxyl radicals and superoxide anions to participate in the degradation of pollutants. In this process, the recombination of electrons and holes is the main reason that leads to the decrease in catalyst activity. The positively charged ions generated by the ionization of cationic dye MB in water can attract electrons and thus reduce the recombination of electron holes. Therefore, the catalyst has always maintained high activity during the five cycles of degradation of MB. However, the negatively charged ions formed by the ionization of anionic dye CR in water repel electrons and make them more prone to hole recombination. Due to the wide band gap of CaWO_4 , electrons will not easily recombine with holes even if there is negative ion repulsion. Therefore, the catalyst can still maintain high activity in the first three cycles of CR degradation experiments. However, under continuous repulsion, the performance of the catalyst will weaken rapidly once the electrons and holes recombine, because the recombination of the electron–hole will significantly reduce the active species in the reaction system. Therefore, the activity of the catalyst decreased significantly in the last two cycles of CR degradation experiments.

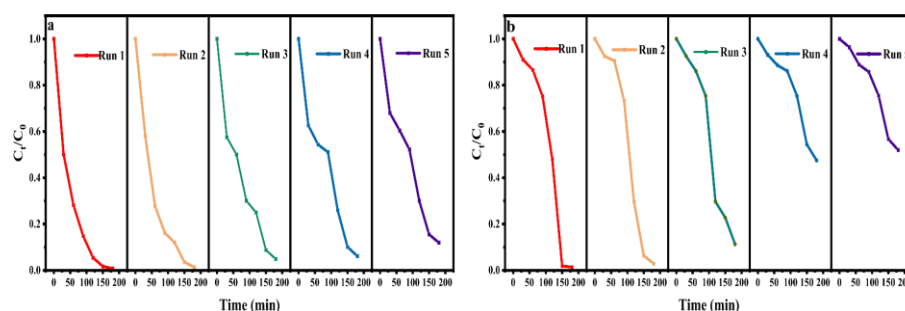


Figure 7. (a) Reusability test on the CaWO_4 degrades MB system, and (b) Reusability test on the CaWO_4 degrades CR system. Reaction conditions: light intensity = 80 W; [MB] = 100 mg/L; and pH = 8.2; [CaWO_4] = 1.0 g/L for (a) and light intensity = 80 W; [CR] = 100 mg/L; pH = 8.2; and [CaWO_4] = 1.0 g/L for (b).

4. Conclusions

In this study, nanoscale- CaWO_4 material was prepared by one-step coprecipitation and then utilized for photo-degradation of MB and CR under UV irradiation. The synthesized nanoparticle material is equipped with a high specific surface area and strong absorption ability under ultraviolet light. Under the same reaction conditions as solid–liquid ratio, light intensity, and pollutant concentration, the pH value difference has the main impact on the optimum conditions for the degradation of MB and CR. For MB, the optimizing condition was a pH of 8.2, while for CR, the optimizing pH was 6. The other reaction

conditions are similar. When the solid–liquid ratio of the catalyst was 1.0 g/L and the light intensity was 60 W, the photocatalytic degradation of 100 mg/L MB and CR can be almost complete. Then, during the reaction, the degradation of both dyes is responsible for different ROS. Holes and hydroxyl radicals are mainly responsible for the degradation of MB while hydroxyl radicals and superoxide anions dominate the degradation of CR. In addition, superoxide anions contribute little to the degradation of MB, holes contribute little to the degradation of CR, and electrons almost do not participate in the degradation of these two dyes. However, due to the difference in dye properties, the stability of the catalyst in degrading MB was better than that in degrading CR.

This study explored a new idea of using a simple method to synthesize mineral-like materials as catalysts to degrade dye wastewater.

Supplementary Materials: The following supporting information can be downloaded at: <https://www.mdpi.com/article/10.3390/pr11041050/s1>, Figure S1a: the Calcium tungstate preparation process diagram; Figure S1b: the Calcium tungstate preparation process schematic diagram; Figure S2: the temperature of the solution during the reaction process; Figure S3: calculation of element proportion; Figure S4a: nitrogen adsorption-desorption isotherms of CaWO₄; Figure S4b: pore size distribution of CaWO₄; Figure S5: photocatalytic degradation of MB by comparison experiments; Figure S6: TOC removal efficiency in photocatalytic degradation of MB; Figure S7: UV–vis spectra in the course of photocatalytic degradation MB; Figure S8: photocatalytic degradation of CR by comparison experiments; Figure S9: TOC removal efficiency in photocatalytic degradation of CR; Figure S10: potential of CaWO₄ solution at different pH values; Figure S11: UV–vis spectra in the course of photocatalytic degradation.

Author Contributions: C.Y.: Conceptualization Ideas, Methodology, Formal analysis, Investigation, Writing. F.S.: Writing—Review and Editing. H.L.: Writing—Review and Editing. T.C.: Supervision, Project administration. Z.C.: Methodology, Formal analysis. H.W.: Methodology, Formal analysis. X.Z.: Writing—Review and Editing. P.Z.: Methodology, Formal analysis. D.C.: Funding acquisition, Writing—Review and Editing. All authors have read and agreed to the published version of the manuscript.

Funding: This study was financially supported by the Anhui Provincial Natural Science Foundation (2208085MD99) and the Hefei Municipal Natural Science Foundation (2022023).

Data Availability Statement: All data generated or analyzed during this study are included in this published article.

Conflicts of Interest: The authors declare no conflict of interest.

References

1. Garg, A.; Chopra, L. Dye Waste: A significant environmental hazard. *Mater. Today* **2022**, *48*, 1310–1315. [[CrossRef](#)]
2. Verma, S.; Rao, B.T.; Singh, R.; Kaul, R. Photocatalytic degradation kinetics of cationic and anionic dyes using Au–ZnO nanorods: Role of pH for selective and simultaneous degradation of binary dye mixtures. *Ceram. Int.* **2021**, *47*, 34751–34764. [[CrossRef](#)]
3. Shabir, M.; Yasin, M.; Hussain, M.; Shafiq, I.; Akhter, P.; Nizami, A.; Jeon, B.; Park, Y. A review on recent advances in the treatment of dye-polluted wastewater. *J. Ind. Eng. Chem.* **2022**, *112*, 1–19. [[CrossRef](#)]
4. Kruusma, J.; Mould, N.; Jurkschat, K.; Crossley, A.; Banks, C.E. Single walled carbon nanotubes contain residual iron oxide impurities which can dominate their electrochemical activity. *Electrochem. Commun.* **2007**, *9*, 2330–2333. [[CrossRef](#)]
5. Zhou, C.; Lai, C.; Huang, D.; Zeng, G.; Zhang, C.; Cheng, M.; Hu, L.; Wan, J.; Xiong, W.; Wen, M.; et al. Highly porous carbon nitride by supramolecular preassembly of monomers for photocatalytic removal of sulfamethazine under visible light driven. *Appl. Catal. B Environ.* **2018**, *220*, 202–210. [[CrossRef](#)]
6. Baklanova, I.V.; Zhukov, V.P.; Krasil'nikov, V.N.; Gyrdasova, O.I.; Buldakova, L.Y.; Shalaeva, E.V.; Polyakov, E.V.; Kuznetsov, M.V.; Shein, I.R.; Vovkotrub, E.G. Fe and C doped TiO₂ with different aggregate architecture: Synthesis, optical, spectral and photocatalytic properties, first-principle calculation. *J. Phys. Chem. Solids* **2017**, *111*, 473–486. [[CrossRef](#)]
7. Li, L.; Yang, X.; Xie, C.; Wang, Y.; Wei, L.; Yang, J. Synthesis and photocatalytic mechanism of visible-light-driven Ag/AgBr/(I/S) composites for organic dyes degradation. *Opt. Mater.* **2022**, *123*, 111947. [[CrossRef](#)]
8. Tian, Y.; Gao, Y.; Wang, Q.; Wang, Z.; Guan, R.; Shi, W. Potassium gluconate-cooperative pore generation based on g-C₃N₄ nanosheets for highly efficient photocatalytic hydrogen production and antibiotic degradation. *J. Environ. Chem. Eng.* **2022**, *10*, 107986. [[CrossRef](#)]

9. Benz, D.; Bui, H.V.; Hintzen, H.T.; Kreutzer, M.T.; Ommen, J.R. Mechanistic insight into the improved photocatalytic degradation of dyes for an ultrathin coating of SiO₂ on TiO₂ (P25) nanoparticles. *Chem. Eng. J.* **2022**, *10*, 100288. [[CrossRef](#)]
10. Wang, M.; Liu, J.; Xu, C.; Feng, L. Sonocatalysis and sono-photocatalysis in CaCu₃Ti₄O₁₂ ceramics. *Ceram. Int.* **2022**, *48*, 11338–11345. [[CrossRef](#)]
11. Hu, X.; Sun, Z.; Song, J.; Zhang, G.; Li, C.; Zheng, S. Synthesis of novel ternary heterogeneous BiOCl/TiO₂/sepiolite composite with enhanced visible-light-induced photocatalytic activity towards tetracycline. *J. Colloid Interface Sci.* **2019**, *533*, 238–250. [[CrossRef](#)]
12. Jia, Z.; Li, T.; Zheng, Z.; Zhang, J.; Liu, J.; Li, R.; Wang, Y.; Zhang, X.; Wang, Y.; Fan, C. The BiOCl/diatomite composites for rapid photocatalytic degradation of ciprofloxacin: Efficiency, toxicity evaluation, mechanisms and pathways. *Chem. Eng. J.* **2020**, *380*, 122422. [[CrossRef](#)]
13. Papoulis, D. Halloysite based nanocomposites and photocatalysis: A Review. *Appl. Clay Sci.* **2019**, *168*, 164–174. [[CrossRef](#)]
14. Gao, H.; Wang, S.; Wang, Y.; Yang, H.; Fang, L.; Chen, X.; Yi, Z.; Li, D. Fabrication and Characterization of BaMoO₄-Coupled CaWO₄ Heterojunction Micro/Nanocomposites with Enhanced Photocatalytic Activity Towards MB and CIP Degradation. *J. Electron. Mater.* **2022**, *51*, 5230–5245. [[CrossRef](#)]
15. Shimi, A.K.; Parvathiraj, C.; Kumari, S.; Dalal, J.; Kumar, V.; Wabaidur, S.M.; Alothman, Z.A. Green synthesis of SrO nanoparticles using leaf extract of Albizia julibrissin and its recyclable photocatalytic activity: An eco-friendly approach for treatment of industrial wastewater. *Environ. Sci. Adv.* **2022**, *5*, 597–866.
16. Chen, Z.; Gong, Q.; Zhu, J.; Yuan, Y.P.; Qian, L.W.; Qian, X.F. Controllable synthesis of hierarchical nanostructures of CaWO₄ and SrWO₄ via a facile low-temperature route. *Mater. Res. Bull.* **2009**, *44*, 45–50. [[CrossRef](#)]
17. Duklan, N.; Chamoli, P.; Raina, K.K.; Shukla, R.K. Effect of UV light irradiation, pH and concentration on the dye sequestration efficiency of anionic surfactant based self-assembled aqueous mesophases. *Surf. Interfaces* **2022**, *28*, 101629. [[CrossRef](#)]
18. Farsi, H.; Barzgari, Z.; Askari, S.Z. Sunlight-induced photocatalytic activity of nanostructured calcium tungstate for methylene blue degradation. *Res. Chem. Intermed.* **2015**, *41*, 5463–5474. [[CrossRef](#)]
19. Zhang, Y.; Fan, R.; Zhang, Q.; Chen, Y.; Sharifi, O.; Leszczynska, D.; Zhang, R.; Dai, Q. Synthesis of CaWO₄-biochar nanocomposites for organic dye removal. *Mater. Res. Bull.* **2019**, *110*, 169–173. [[CrossRef](#)]
20. Zhang, Y.; Zhang, L.; Kang, L.; Yang, M.; Zhang, K. A new CaWO₄/alkali-activated blast furnace slag-based cementitious composite for production of hydrogen. *Int. J. Hydrogen Energy* **2017**, *42*, 3690–3697. [[CrossRef](#)]
21. Wen, D.; Li, W.; Lv, J.; Qiang, Z.; Li, M. Methylene blue degradation by the VUV/UV/persulfate process: Effect of pH on the roles of photolysis and oxidation. *J. Hazard. Mater.* **2020**, *391*, 121855. [[CrossRef](#)] [[PubMed](#)]
22. Nguyen, C.H.; Fu, C.; Juang, R. Degradation of methylene blue and methyl orange by palladium-doped TiO₂ photocatalysis for water reuse: Efficiency and degradation pathways. *J. Clean. Prod.* **2018**, *202*, 413–427. [[CrossRef](#)]
23. Wen, X.; Tang, L. One-dimensional copolymer nanostructures loaded with silver nanoparticles fabricated via metallogel template copolymerization and their pH dependent photocatalytic degradation of methylene blue. *J. Mol. Catal. A Chem.* **2015**, *399*, 86–96. [[CrossRef](#)]
24. Kedves, E.; Bárdos, E.; Gyulavári, T.; Pap, Z.; Hernadi, K.; Baia, L. Dependence of cationic dyes' adsorption upon α-MoO₃ structural properties. *Appl. Surf. Sci.* **2022**, *573*, 151584. [[CrossRef](#)]
25. Guo, R.; Wang, J.; Bi, Z.; Chen, X.; Hu, X.; Pan, W. Recent advances and perspectives of g-C₃N₄-based materials for photocatalytic dyes degradation. *Chemosphere* **2022**, *295*, 133834. [[CrossRef](#)]
26. Sun, F.; Chen, T.; Liu, H.; Zou, X.; Zhai, P.; Chu, Z.; Shu, D.; Wang, H.; Chen, D. The pH-dependent degradation of sulfadiazine using natural siderite activating PDS: The role of singlet oxygen. *Sci. Total Environ.* **2021**, *784*, 147117. [[CrossRef](#)]
27. Zhou, Y.; Zhang, D.; Pan, J.; Kong, X.; Liu, Y.; Sun, L.; Wang, L.; Li, D. Overexpression of a multiple stress-responsive gene, ZmMPK4, enhances tolerance to low temperature in transgenic tobacco. *Plant Physiol. Biochem.* **2012**, *58*, 174–181. [[CrossRef](#)] [[PubMed](#)]
28. Xia, M.; Liu, H.; Wang, H.; Sun, F.; Zou, X.; Chen, T.; Chu, Z.; Chen, D.; Zhou, Y.; Xie, Q. Impact of the interaction between hematite and halloysite on environmental fate of organic pollutants. *Appl. Clay Sci.* **2021**, *209*, 106123. [[CrossRef](#)]
29. Othman, I.; Mohamed, R.M.; Ibrahim, F.M. Study of photocatalytic oxidation of indigo carmine dye on Mn-supported TiO₂. *J. Photochem. Photobiol. A* **2007**, *189*, 80–85. [[CrossRef](#)]
30. Sahel, K.; Perol, N.; Dappozze, F.; Bouhent, M.; Derriche, Z.; Guillard, C. Photocatalytic degradation of a mixture of two anionic dyes: Procion Red MX-5B and Remazol Black 5 (RB5). *J. Photochem. Photobiol. A* **2010**, *212*, 107–112. [[CrossRef](#)]
31. Barka, N.; Assabane, A.; Nounah, A.; Ichou, Y.A. Photocatalytic degradation of indigo carmine in aqueous solution by TiO₂-coated non-woven fibres. *J. Hazard. Mater.* **2008**, *152*, 1054–1059. [[CrossRef](#)] [[PubMed](#)]
32. Thiam, A.; Brillas, E.; Centellas, F.; Cabot, P.L.; Sirés, I. Electrochemical reactivity of Ponceau 4R (food additive E124) in different electrolytes and batch cells. *Electrochim. Acta* **2015**, *173*, 523–533. [[CrossRef](#)]
33. Li, K.; Dong, C.; Zhang, Y.; Wei, H.; Zhao, F.; Wang, Q. Ag–AgBr/CaWO₄ composite microsphere as an efficient photocatalyst for degradation of Acid Red 18 under visible light irradiation: Affecting factors, kinetics and mechanism. *J. Mol. Catal. A Chem.* **2014**, *394*, 105–113. [[CrossRef](#)]
34. Jayakrishnan, C.; Sheeja, S.R.; Duraimurugan, J.; Prabhu, S.; Ramesh, R.; Kumar, G.S.; Subhash, K.G.; Shkir, M.; Pallavolu, M.R. Synthesis of dumbbell-shaped ZnO nanostructures for energy storage and photocatalytic dye degradation applications. *Mate Technol.* **2022**, *37*, 3006–3016. [[CrossRef](#)]

35. Sampath, S.; Rohini, V.; Chinnasamy, K.; Ponnusamy, P.; Thangarasau, S.; Kim, W.K.; Reddy Minnam Reddy, V.; Shkir, M.; Maiz, F. Solvothermal synthesis of magnetically separable Co–ZnO nanowires for visible light driven photocatalytic applications. *Phys. B* **2023**, *652*, 414654. [[CrossRef](#)]
36. Atran, A.A.; Ibrahim, F.A.; Awwad, N.S.; Shkir, M.; Hamdy, M.S. Facial One-Pot Synthesis, Characterization, and Photocatalytic Performance of Porous Ceria. *Catalysts* **2023**, *13*, 240. [[CrossRef](#)]
37. Ranjith, R.; Vignesh, S.; Balachandar, R.; Suganthi, S.; Raj, V.; Ramasundaram, S.; Sundar, J.K.; Shkir, M.; Oh, T.H. Construction of novel g-C₃N₄ coupled efficient Bi₂O₃ nanoparticles for improved Z-scheme photocatalytic removal of environmental wastewater contaminant: Insight mechanism. *J. Environ. Manag.* **2023**, *330*, 117134. [[CrossRef](#)]
38. Li, J.; Zhou, Z.; Li, X.; Yang, Y.; Gao, J.; Yu, R.; Wang, H.; Wang, N. Synergistically boosting sulfamerazine degradation via activation of peroxydisulfate by photocatalysis of Bi₂O₃-TiO₂/PAC under visible light irradiation. *Chem. Eng. J.* **2022**, *428*, 132613. [[CrossRef](#)]
39. Syed, A.; Al-Shwaiman, H.A.; Al Khulaifi, M.M.; Al Zahrani, R.R.; Almajhdi, F.N.; Elgorban, A.M. Integrating plasmonic effect and nano-heterojunction formation for boosted light harvesting and photocatalytic performance using CaWO₄/Ag₂MoO₄ and its antibacterial applications. *Mat. Sci. Semicond. Proc.* **2021**, *133*, 105921. [[CrossRef](#)]
40. Ayappan, C.; Palanivel, B.; Jayaraman, V.; Maiyalagan, T.; Mani, A. One-step hydrothermal synthesis of CaWO₄/α-Ag₂WO₄ heterojunction: An efficient photocatalyst for removal of organic contaminants. *Mat. Sci. Semicond. Proc.* **2019**, *104*, 104693. [[CrossRef](#)]
41. Mahendra, K.; Fernandes, J.M.; Fernandes, B.J.; Bindu, K.; Ramesh, K.P. Photocatalytic degradation of organic textile dyes using tellurium-based metal alloy. *Vacuum* **2022**, *199*, 110960.
42. Zhai, P.; Liu, H.; Sun, F.; Chen, T.; Zou, X.; Wang, H.; Chu, Z.; Wang, C.; Liu, M.; Chen, D. Carbonization of methylene blue adsorbed on palygorskite for activating peroxydisulfate to degrade bisphenol A: An electron transfer mechanism. *Appl. Clay Sci.* **2022**, *216*, 106327. [[CrossRef](#)]
43. Zhu, Y.; Wang, F.; Zhou, B.; Chen, H.; Yuan, R.; Zhang, Y.; Geng, H.; Liu, Y.; Wang, H. Photo-assisted Fe²⁺ modified molybdenum disulfide activated potassium persulfate to degrade sulfadiazine: Insights into the degradation pathway and mechanism from density functional theory. *Chem. Eng. J.* **2022**, *435*, 134904. [[CrossRef](#)]

Disclaimer/Publisher's Note: The statements, opinions and data contained in all publications are solely those of the individual author(s) and contributor(s) and not of MDPI and/or the editor(s). MDPI and/or the editor(s) disclaim responsibility for any injury to people or property resulting from any ideas, methods, instructions or products referred to in the content.